

Received January 6, 2021, accepted January 20, 2021, date of publication February 1, 2021, date of current version February 8, 2021.

Digital Object Identifier 10.1109/ACCESS.2021.3055807

# Reverse Procedure Detection of Space Target Streaks Based on Motion Parameter Estimation

YUNLONG ZOU<sup>1,2</sup>, JINYU ZHAO<sup>1</sup>, YUANHAO WU<sup>1</sup>, BIN WANG<sup>1</sup>, AND LEI DONG<sup>1</sup>

<sup>1</sup>Changchun Institute of Optics, Fine Mechanics and Physics, Chinese Academy of Sciences, Changchun 130033, China

<sup>2</sup>University of Chinese Academy of Sciences, Beijing 100049, China

Corresponding author: Jinyu Zhao (zhaojy@ciomp.ac.cn)

This work was supported in part by the Joint Fund of Astronomy of the National Natural Science Foundation of China under Grant U1831106, and in part by the Third Phase of Innovative Engineering Projects of the Changchun Institute of Optics, Fine Mechanics and Physics, Chinese Academy of Sciences, under Grant 065X32CN60.

**ABSTRACT** This paper proposes a reverse procedure detection method for space target streaks based on motion parameter estimation. According to the phase shift characteristics of the spectrum, the interframe phase difference is used to obtain the displacement vectors of the target streak and image background, and then the morphological parameters of the target streak are estimated. In addition, a streak window is designed on the basis of the parameters, utilizing the local grayscale correlation in two image frames to carry out target searching and positioning with the interval of the target displacement vector. Images from different scenes are used to evaluate the adaptability of our method, and the experimental results suggest that the expected targets can be detected successfully with subpixel precision in all telescope operating modes. The proposed frequency-domain reverse procedure detection method avoids the problem of fake target confirmation caused by blind detection in traditional methods and overcomes the interference produced when the target streak passes through a bright star. Moreover, first target tracking and then positioning, which cannot be performed with time-domain methods, can be achieved. Our proposed method is attractive for multiple applications, such as space target cataloging, early warning and orbit prediction.

**INDEX TERMS** Reverse procedure detection, motion parameter estimation, morphological parameter estimation, local correlation positioning.

## I. INTRODUCTION

Space target detection techniques are important for aerospace safety and space early warnings. Several methods have been used for target detection. Background difference algorithms [1]–[4] need to accurately model the image background and update it constantly; these algorithms are accurate and easy to implement but are greatly affected by changes in illumination, scene complexity and noise. In interframe difference algorithms [5]–[7], one of the two frames is taken as the background, and interframe registration and threshold selection are implemented. These algorithms are simple and stable, but the extraction of object regions is not complete, and the detection results are affected by the selection of the interframe time intervals. The optical flow method [8]–[10] aims to analyze optical field changes in local regions in the time domain, and target detection can be carried out without

any scene information. However, due to the complexity of the calculations and poor real-time performance, target motion estimation is generally realized with a combination of other methods.

The image characteristics in the spatial domain are also crucial information. Filter-based algorithms [11]–[14] are designed based on the gray distribution difference between the target region and background, and they are sensitive to the clutter background. Matched filter algorithms [15], [16] have advantages in searching for a specific target with the target template, but for targets with no prior information, the efficiency of target searching is low. The point spread function (PSF) fitting method [17] is required to establish a target model with Gaussian functions, yet it has poor adaptability to different targets. Deconvolution techniques [18]–[21] offer a direct approach to mitigate the effects of extended and irregular PSFs and to upgrade the image quality of a point source. However, these techniques are affected by the noise and prior knowledge of targets. Morphology-based

The associate editor coordinating the review of this manuscript and approving it for publication was Marco Martalo<sup>1</sup>.

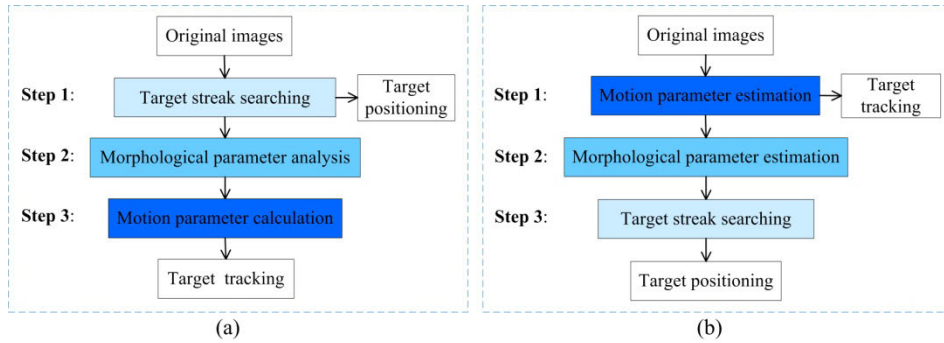


FIGURE 1. Comparison of target detection procedures. (a) Traditional procedure. (b) Our procedure.

methods [6], [22]–[26] are used to discriminate the morphological characteristics of regions of interest, but there are some limitations for targets that are partially discontinuous in complex backgrounds.

The traditional methods conduct blind detection of targets based on the local gray features [27], [28] of the image, and fake targets must be removed without prior knowledge of the targets. The core of the detection procedure is to locate the target first and then calculate motion information, whereas the global features of the image are ignored.

Global motion [29] can be estimated from the local motions of subimages, which are detected based on phase correlation. Wu and Yu [30] proposed a new algorithm for estimating the motions of the target and image background by Fourier transform. The algorithm focuses on the global features of images and analyzes the interframe phase variation, but target detection is not carried out. Our proposed method conducts space target streak detection based on movement estimation. We utilize the target displacement vector to accurately estimate the morphological parameters of the target streak, and the target is located based on the local gray level correlation between two frames without interframe registration and local feature analysis. Our method executes a procedure of first estimating target motion and then positioning, which is a new idea for target detection.

II. DETECTION PROCEDURE AND ALGORITHMS

The traditional target detection procedure and our proposed detection procedure are obviously different, as shown in Fig. 1. In traditional methods, it is crucial that the target streak is recognized first, and the morphological parameters of the target streak are analyzed for interframe matching to obtain the target motion parameters. However, our idea is to obtain the target motion parameters first by interframe phase difference, then the morphological parameters of the target streak are estimated to carry out target positioning; thus, the steps are completely reversed.

A. ADVANTAGES OF REVERSE PROCEDURE DETECTION

A schematic diagram of reverse procedure detection (RPD) is shown in Fig. 2, and we summarize the following advantages.

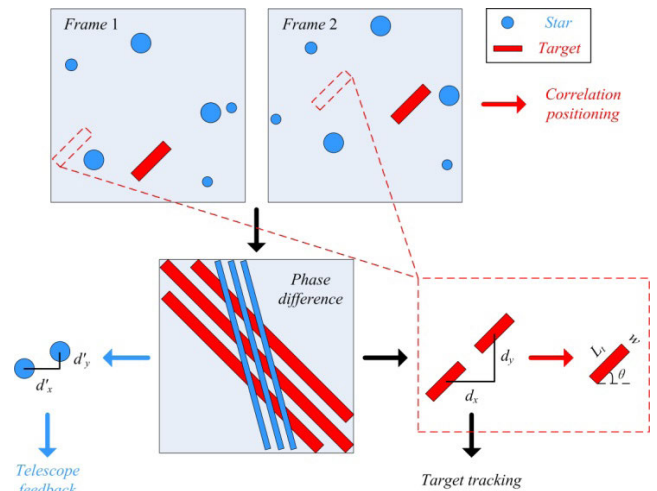


FIGURE 2. A schematic diagram of reverse procedure detection is displayed. The phase difference, obtained first, is used to obtain the star displacement for motion feedback of the telescope and the target displacement for target tracking, searching and positioning.

1) TRACKING WITHOUT POSITIONING

We obtain the target displacement by using the phase difference between two images, which means that the optical telescope can be directly guided by the interframe displacement to fix the target at one certain position in the field of view even though we have no information about the target. This achieves target tracking without target positioning.

2) MULTITARGET STATUS MONITORING

Suspicious targets in the field of view are cataloged in real time and monitored automatically by detecting the target pulse peaks in the Fourier spectrum of the phase difference, and the space target monitoring system alarms immediately when the same target peak occurs continuously.

3) SEARCHING WITH MORPHOLOGICAL PARAMETERS

We accurately estimate the morphological parameters of the target streak with the target displacement vector. Searching for a target with a known target shape is superior to blind detection.

4) ROBUSTNESS TO INTERFERENCE FROM BRIGHT STARS

We design two identical streak windows on the basis of target morphology for gray correlation searching to obtain the correlation coefficient matrix and conduct target positioning by calculating the center of the maximum peak in the correlation coefficient matrix. Even though the peak may be disturbed by bright stars, we can find the affected location of the peak based on its outline and repair it with the theoretical form that we estimate accurately.

B. TARGET DISPLACEMENT VECTOR ESTIMATION

Two consecutive frames of images are taken from an image sequence. If there is a target displacement, there is a corresponding phase shift in the frequency domain. Assuming that the target moves a distance of ‘a’ in the direction of the X-axis and ‘b’ in the direction of the Y-axis, the phase difference between the two frames of images [31] can be expressed as

$$\vartheta_{\Delta}(u, v) = \vartheta_2(u, v) - \vartheta_1(u, v) = 2\pi(au + bv) \quad (1)$$

The phase difference spectrum is shown as a bright and dark fringe with a period of  $2\pi$ , and the periodic numbers in the X-axis and Y-axis represent the distance of movement in both directions. After the unit amplitude spectrum of the phase difference is taken to form a new spectrum, the Fourier transform is applied to obtain a pulse peak whose coordinates correspond to the target displacement between the two frames, as follows.

$$F(x, y) = \mathcal{F}\{\exp[-j2\pi(af_x + bf_y)]\} = \delta(x - a, y - b) \quad (2)$$

If there are several targets with the same status of motion in the image sequence, the number of pulse peaks does not increase, but the amplitude rises.

C. TARGET MORPHOLOGICAL PARAMETER ESTIMATION

By detecting pulse peaks, we obtain the displacement vectors of the image background and the target, which are  $(a_0, b_0)$  and  $(a_1, b_1)$ , respectively, and the image background velocity in the image sequence can be calculated as

$$V_0 = \left(a_0^2 + b_0^2\right)^{1/2} / T_0 \quad (3)$$

where  $T_0$  is the time interval between two frames, and the value of the background velocity is matched with the Earth rotation rate and telescope movement rate to distinguish the peaks of the target and background.

There are two types of target velocities,

$$V_1 = \left((a_1 - a_0)^2 + (b_1 - b_0)^2\right)^{1/2} / T_0 \quad (4)$$

$$V_2 = \left(a_1^2 + b_1^2\right)^{1/2} / T_0 \quad (5)$$

where  $V_1$  is the target velocity relative to stars and  $V_2$  is the target interframe velocity. We can estimate the direction of the target streak,

$$\theta = -\arctan(b_1/a_1) \quad (6)$$

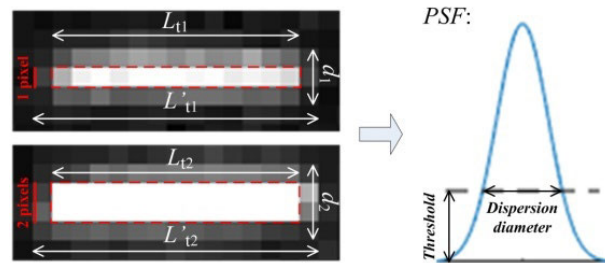


FIGURE 3. Estimation model of the target dispersion diameter.

where  $\theta$  is the angle from the positive direction of the X-axis to the direction of the tilting target streak, with the counterclockwise direction defined as positive. The target interframe velocity  $V_2$  and the exposure time  $T_{exp}$  are used to estimate the theoretical length of the target streak  $L_t$ , which is the number of pixels that the center of the point target travels within the exposure time.

$$L_t = V_2 \cdot T_{exp} \quad (7)$$

D. EFFECT OF DISPERSION ON PARAMETER ESTIMATION

Considering the imaging characteristics of optical systems, stars and space targets appear as approximately symmetric Gaussian distributions, and bright spots diffuse to the surroundings [32]–[35]. In a certain exposure time, the target extends in the direction of motion and its energy diffuses to multiple adjacent pixels. The estimation model of the target dispersion diameter is shown in Fig. 3.

We select a threshold above the background intensity, and the bright spot width corresponding to the threshold is the dispersion diameter. The threshold is selected based on the proportion of energy above the threshold to the total energy, or the maximum gray value of a certain percentage can be selected by experience as the threshold. Generally, the dispersion spot of a dark streak is small, and its center occupies one or two lines of pixels; thus, for the two types of target streaks, the lengths under dispersion can be expressed as

$$L'_{t1} = L_{t1} + (d_1 - 1) / \cos \theta_1 \quad (8a)$$

$$L'_{t2} = L_{t2} + (d_2 - 2) / \cos \theta_2 \quad (8b)$$

For both types of target streaks, dispersion diameters  $d_1$  and  $d_2$  are approximately 3 and 4, so the length can be rewritten as

$$L'_t = L_t + 2 / \cos \theta \quad (9)$$

At this point, the length, width, inclined direction and displacement of the target streak have been obtained.

E. EFFECT OF BRIGHT STARS ON LOCAL GRAY CORRELATION POSITIONING

Two identical rectangular windows of length  $L'_t$ , diffusion width  $d$ , and inclined direction  $\theta$  are selected for local grayscale correlation in the two frames, and the interval of the two windows is the target interframe displacement vector

$(a_1, b_1)$ . We take them for traversal in the images to obtain the correlation coefficient matrix. In theory, the center of the maximum peak in the matrix is the location of the target, whose length is computed as

$$L_p = L'_t + L_{real} - 1/\cos\theta \quad (10)$$

Nevertheless, when the target streak approaches a bright star in the direction of motion, the maximum peak is truncated, and its length  $L_p$  is inaccurate. Therefore, we have to estimate it with the theoretical streak length,

$$L'_p = 2L'_t - 1/\cos\theta \quad (11)$$

We can compare the real length of the peak with the theoretical length in the correlation coefficient matrix to judge whether there is interference from a bright star. If there is no interference, both are almost the same, and we can directly use the real peak for accurate target positioning. Otherwise, the outline of the peak is analyzed to find the affected position and complement it. A positioning error is produced when taking the center of the complete peak for positioning, and the positioning accuracy can be defined as

$$\Delta L_{center} = (L'_p - L_p) / 2 = (L'_t - L_{real}) / 2 \quad (12)$$

### III. EXPERIMENTAL RESULTS AND ANALYSIS

We conduct fifty groups of experiments in three different scenes to evaluate the effectiveness of the proposed RPD method. All working modes of the telescope, keeping still, following targets and following stars, are included in the three scenes, and the motion parameters and morphological parameters of the target streaks are different. First, we estimate the target displacement with the interframe phase difference spectrum. Second, we carry out target parameter analysis based on the target displacement vectors. Finally, we implement target positioning with local gray correlation to show the effectiveness of our method.

In the experiments, we calculate the barycenter of the pulse peaks in the spectrum to determine the target displacement, and the mean value of the maximum peak in the correlation coefficient matrix is taken for the streak center positioning. The error standard  $\sigma$  used in the length estimation is one pixel.

#### A. EXPERIMENTAL SETUP

The star images used in our work were acquired by the Chinese Academy of Sciences Ground-based Optical Telescope with a large field of view ( $3.2^\circ$ ). Affected by the working modes of the telescope, the exposure time and the velocities of the targets, the lengths of the selected star image sequences containing different target streaks are different. In Sequence 1, the target streak remains in the field of view for forty frames. Sequence 2 consists of only three frames because the working mode of the telescope changed after target detection. Sequence 3 comprises ten frames because the telescope was switched to observe a new target. We took the first two frames of each sequence as examples to analyze

the estimation accuracies for the target parameters and ran our approach in MATLAB 2016a. The overall algorithm of RPD is summarized below.

---

#### Algorithm 1 Overall Algorithm of RPD

---

**Input:** two consecutive frames of images,  $Im_1(x, y)$  and  $Im_2(x, y)$

**Output:** the position of target streak center,  $(p_x, p_y)$

- 1: Calculate interframe phase difference  $\Phi_\Delta(u, v)$  according to (1).
  - 2: Obtain target displacement vector  $(a, b)$  by using (2).
  - 3: Use (3)-(11) to estimate the streak parameters  $\theta, L'_t, d,$  and  $L'_p$ .
  - 4: Design two identical streak windows  $W_1$  and  $W_2$  with parameters  $L'_t, d,$  and  $\theta$  in  $Im_1(i, j)$  and  $Im_2(i + a, j + b)$ , respectively.
  - 5: **for** every effective  $(i, j)$
  - 6:   Use the correlation coefficient of  $W_1$  and  $W_2$  to update the correlation coefficient matrix  $corrMatrix(i, j)$ .
  - 7: **end for**
  - 8: Find the maximum peak of  $corrMatrix$  to calculate the length  $L_p$  and the peak center  $(p_x, p_y)$ .
  - 9: **if**  $abs(L_p - L'_p) < 2\sigma$
  - 10:   **return** the position of target steak center  $(p_x, p_y)$
  - 11: **else**
  - 12:   Update  $L_p$  with  $L'_p$ , and calculate the new peak center  $(p'_x, p'_y)$ .
  - 13:   **return** the position of the target streak center  $(p'_x, p'_y)$
  - 14: **end if**
- 

#### B. TARGET DISPLACEMENT DETECTION

Two consecutive frames are selected from each of the three image sequences, and the image sequences represent three specific scenes where the telescope is working in different modes. Three groups of images and interframe phase differences are shown in Fig. 4.

In Scene 1, the optical telescope stands still and points to the sky. Due to the Earth's rotation, the stars are slightly extended in the star images with a 1.6-second exposure time, and the target streak is moving in the lower-left direction. In Scene 2, the telescope is working in staring mode and moves with one certain target that is not displayed in the images. The stars are elongated as horizontal streaks in a 4.6-second exposure time, and the target streak is moving in the upper-right direction. Scene 3 is a still background mode with a 4.8-second exposure time, and the target streak is transverse. There are two types of fringes in the phase difference spectra in Fig. 4(a) and Fig. 4(b). One is a longitudinal fringe generated by the lateral movement of the background, and the other is an inclined fringe generated by the movement of the target. In Fig. 4(c), the vertical fringe is generated by the lateral displacement of the target, whereas the static image background leads to a wide range of zero phase shifts.

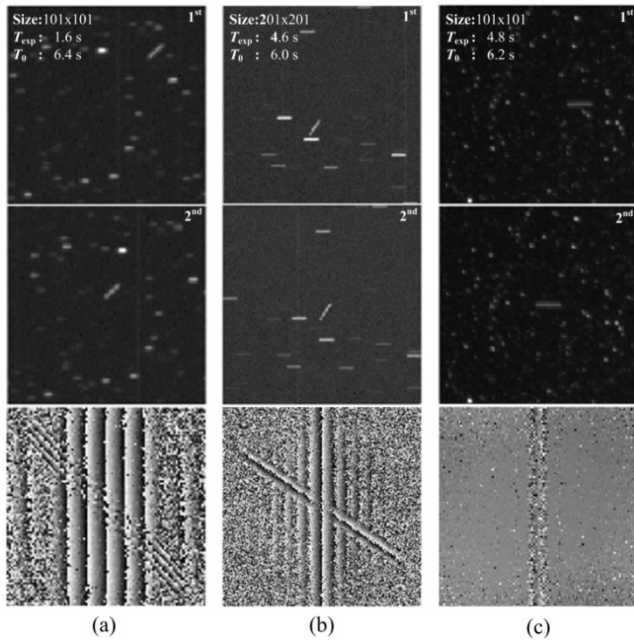


**FIGURE 4.** Two frames of images and interframe phase differences in different scenes. (a) Scene 1: the telescope stands still, and the target moves down and left. (b) Scene 2: the telescope follows one certain target, and a new target streak moves up and right. (c) Scene 3: the telescope follows stars, and the target moves left.

The results of the Fourier transform after taking the unit amplitude spectra of the phase differences are shown in Fig. 5. Each spectrum has two peaks representing the target and background, and the barycenters of each peak are taken to obtain the pulse coordinates. The coordinates are the displacements of the target streak and image background. The error of the barycenter produced by different threshold values is very small and is at the subpixel level.

**C. TARGET PARAMETER ANALYSIS**

The target grayscale curves in the direction of the target streaks in each scene are shown in Fig. 6. The target streak center of Scene 1 spans two pixels in its vertical direction, so the two lines of pixels where the target streak is located are taken from each of the two images to analyze the intensity variation. The target streak centers of Scene 2 and Scene 3 occupy one pixel, so one line of pixels is taken. Similarly, the case will occur in its parallel direction. We find that the target gray curves in the two frames are approximately consistent but sometimes not perfectly matched. In Fig. 6(c), the target lengths in Im1 and Im2 are different, and an error of one pixel is generated. It is inevitable that we can read the intensity only by pixel, so this affects our confirmation of the target length, but this case does not affect the estimation of the target length or target positioning.

The calculation method of the target length in the image is the ratio of the number of pixels that the target streak occupies in its inclined direction to the cosine of the inclination angle. For example, for the streak length in Fig. 6(a),

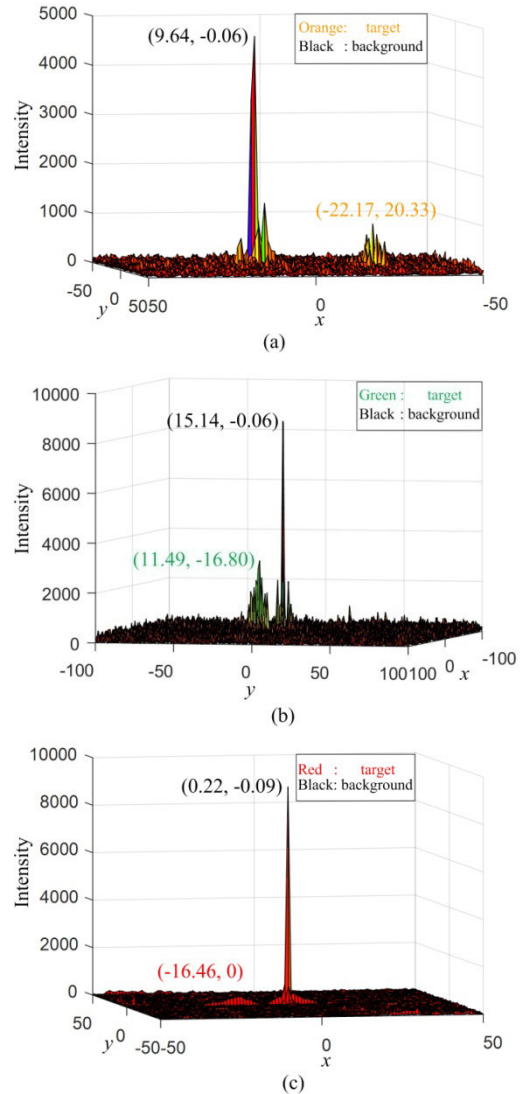


**FIGURE 5.** Fourier transform after taking the unit amplitude spectra of the phase differences. (a) Scene 1: background moves right. (b) Scene 2: background moves right. (c) Scene 3: background is still.

**TABLE 1.** Information on targets and image backgrounds in the three image sequences.

| No. | $V_0$ | $V_1$ | $V_2$ | $\theta$ | $L_t$ | $L'_t$ | $L'_p$ | $L_{im}$ | $L'_{im}$ |
|-----|-------|-------|-------|----------|-------|--------|--------|----------|-----------|
| 1   | 1.5   | 5.95  | 4.7   | 42.5     | 7.5   | 10.2   | 19     | 8.1      | 10.9      |
| 2   | 2.5   | 2.86  | 3.39  | 55.6     | 15.6  | 19.1   | 36.4   | 15.9     | 19.5      |
| 3   | 0.04  | 2.69  | 2.65  | 0        | 12.7  | 14.7   | 28.4   | 12       | 14        |

$L_{im} = 6 / \cos 42.5^\circ = 8.1$ , and  $L'_{im} = 8 / \cos 42.5^\circ = 10.9$  (units: pixel). The information of the target length in the image is obtained, and the relevant information of the targets in each scene is estimated by using (3)-(11), as shown in TABLE 1.

It is found that the target length estimated in theory is very close to the target length in the image and that the error is less than one pixel, which indicates that the target information

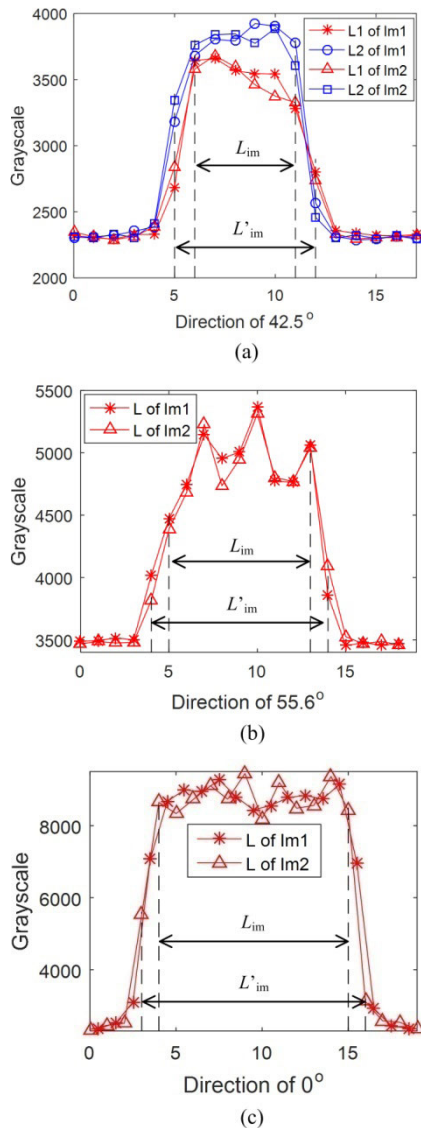


**FIGURE 6.** Grayscale curves of each target streak (centerlines of each target streak:  $L$ ,  $L_1$  and  $L_2$ , two images of each scene:  $Im_1$  and  $Im_2$ , target length:  $L_{im}$ , target length under dispersion:  $L'_{im}$ ). (a) Scene 1: two lines of pixels. (b) Scene 2: one line of pixels. (c) Scene 3: one line of pixels.

estimated in the frequency-domain method in this paper is effective.

**D. TARGET CORRELATION POSITIONING**

Three groups of target windows are designed to obtain the correlation coefficient matrixes on the basis of the target information of  $d$ ,  $\theta$  and  $L'_t$ , and peak compensation and target positioning are carried out, as shown in Fig. 7. Considering the information of the target length, width, and displacement, we can preliminarily exclude invalid locations of the target centers in the first images of each scene and mark the effective regions with red dashed boxes in Fig. 7(b). The direction of the maximum peak in each matrix is the same as that of the target streak. Then, the length and outline of the peaks are analyzed, and it is found that the peak in Scene 2 is

**TABLE 2.** Information on the simulation targets ( $l$ : target length,  $\theta$ : streak angle,  $d$ : displacement vector).

| Parameter             | Tar 1   | Tar 2     | Tar 3     | Tar 4     | Tar 5    |
|-----------------------|---------|-----------|-----------|-----------|----------|
| $l$ (pixel)           | 10      | 11.18     | 14.14     | 11.18     | 10       |
| $\theta$ ( $^\circ$ ) | 0       | 26.565    | 45        | 63.435    | 90       |
| $d$ (pixel)           | (20, 0) | (-20, 10) | (20, -20) | (-10, 20) | (0, -20) |

laterally truncated at the lower edge, which means that there is interference from a bright star below the target streak. We must complement the maximum peak to the theoretical length at its lower edge, whereas the other two peaks are almost the same as the theoretical ones, so we can directly use them, as shown in Fig. 7(c). Finally, the target streak positions obtained by calculating each center of the complete peaks are successfully marked by the red squares in Fig. 7(d).

The target positioning accuracy is half of the estimation accuracy of the target streak length according to (12), i.e., at the subpixel level. We compare the target positions obtained using the RPD method with those in the images, and the real positioning errors that we obtain in each scene are less than one pixel, indicating that our proposed RPD method is effective. In addition, the target can be identified and tracked in the second frame of each sequence. However, there is no way to obtain the true length and position of the target from the star images, and there must be errors in the estimation. Therefore, we carry out a star image simulation experiment to validate the detection performance with metrics, accuracies and false alarms.

**IV. DETECTION PERFORMANCE ANALYSIS**

We simulate five star image sequences of 100 frames each, and the morphological parameters and motion parameters of the target streak in each image sequence are different. Moreover, stars of different intensities, that is, 75, 150 and 255, are placed in random positions of simulation star images, and the numbers are 30, 20 and 10, respectively. The image background intensity and the target center intensity are set to 50 and 200, respectively (we generally cut down the intensity of the bright stars in the real star images to reduce the peak amplitude generated by star interframe displacement). Additionally, we add Gaussian noise of different levels to the images to simulate the image background. Information on the five simulation targets is shown in TABLE 2.

**A. FALSE ALARM ANALYSIS**

In our detection process, the amplitude and shape of the pulse peaks that correspond to the displacement of the target and the stars in the image are two important bases in peak extraction. The amplitude is related to the intensity of the targets or stars, and the amplitude of the interference peaks ranges from 0 to several hundred, whereas the peak value of the target ranges from several hundred to several thousand, and the peak value of the star ranges from several thousand to tens of thousands. Additionally, the shape of the pulse peak generated by the

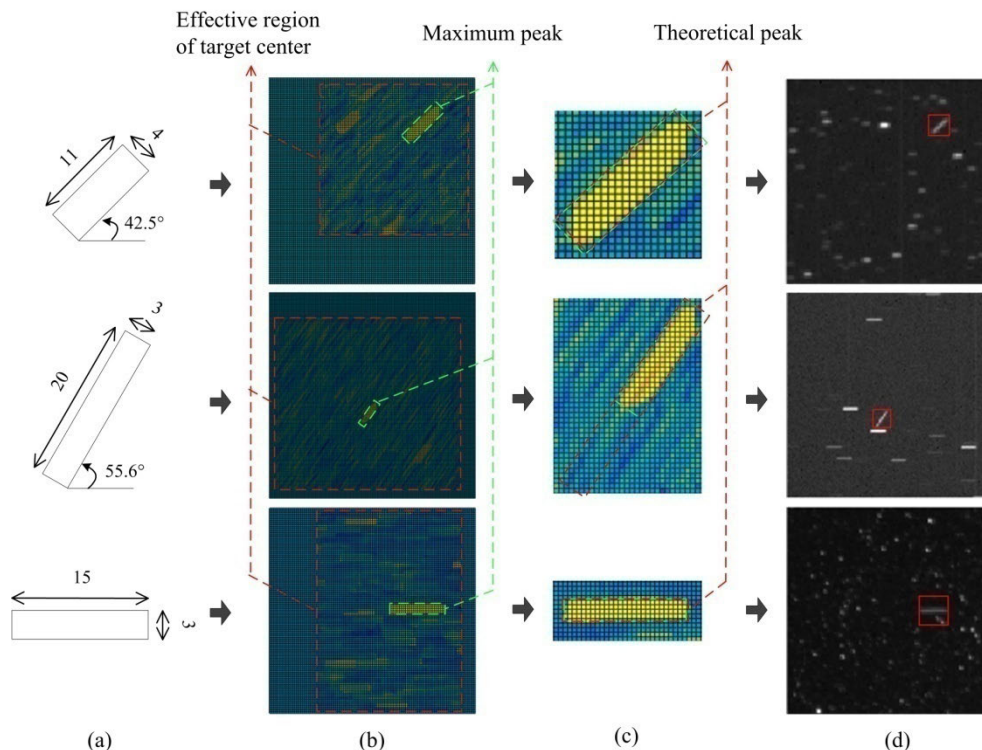


**FIGURE 7.** Target streak detection results in the first frames of each scene. (a) Target searching windows. (b) Correlation coefficient matrices. (c) Peak analysis. (d) Target positioning.

**TABLE 3.** Pulse peak amplitudes at different noise levels (#1: star displacement peak, #2: target displacement peak, #0: mean intensity of interference pulses).

| Noise | Peak no. | Seq 1 | Seq 2 | Seq 3 | Seq 4 | Seq 5 |
|-------|----------|-------|-------|-------|-------|-------|
| 0     | # 1      | 28417 | 28141 | 25089 | 28054 | 28462 |
|       | # 2      | 9874  | 10348 | 13407 | 10454 | 9876  |
|       | # 0      | 86    | 85    | 82    | 86    | 86    |
| 5     | # 1      | 7924  | 8305  | 7930  | 8330  | 8386  |
|       | # 2      | 1465  | 1999  | 2109  | 1553  | 1391  |
|       | # 0      | 152   | 151   | 151   | 152   | 151   |
| 10    | # 1      | 4572  | 4835  | 4755  | 5146  | 4426  |
|       | # 2      | 1091  | 888   | 1034  | 895   | 1126  |
|       | # 0      | 157   | 157   | 156   | 157   | 157   |

target displacement appears as an elongated peak consistent with the direction of the target streak. Therefore, false alarms in the paper mean that we mistake the interference peak as the target displacement peak.

In TABLE 3, we list the pulse peak amplitude of the stars and targets and the average intensity of the interference pulses at different noise levels to analyze false alarms. We find that the target displacement peak is relatively high and very easy to detect. However, with increasing noise intensity, the peak value of the target displacement decreases rapidly and become close to the interference pulse peak, which makes it hard to detect the target peak. In this case, the detection

should be carried out in combination with the peak morphology. Each position has its own unique peak shape, so false alarms can be removed by combining with the shape when multiple suspicious peaks are detected. However, this does not mean that this method can detect the target displacement without false alarms under high noise levels. When the target displacement peak is close to the background intensity, its morphological information is completely lost, so this method cannot work well. Therefore, the problem of false alarms is related to the noise level, target intensity, image size, number of stars and many other factors, and the method in the paper can ensure the detection of target displacement without false alarms at the normal noise level.

**B. ACCURACY ANALYSIS**

The inverse procedure detection method can detect the target displacement, estimate the target parameters and then search for and locate the targets. There are three estimation errors in the process: the displacement estimation error, angle estimation error and length estimation error. The mean value and standard deviation of the detection errors at different noise levels are shown in TABLE 4.

When Gaussian noise with a standard deviation of 5 is added, the detection accuracy of the target displacement is 0.31 pixels, the length estimation accuracy is 0.14 pixels, and the angle estimation accuracy is 0.3°. When Gaussian noise with a standard deviation of 10 is added, the target displacement accuracy is 0.48 pixels, the length estimation accuracy

**TABLE 4.** Estimation accuracy analysis at different noise levels ( $\Delta d$ : displacement estimation error,  $\Delta\theta$ : angle error,  $\Delta l$ : length error,  $m$ : mean,  $\sigma$ : standard deviation).

| Error                          | Noise | Tar 1       |            | Tar 2       |            | Tar 3       |            | Tar 4       |            | Tar 5      |            |
|--------------------------------|-------|-------------|------------|-------------|------------|-------------|------------|-------------|------------|------------|------------|
|                                |       | $m_1$       | $\sigma_1$ | $m_2$       | $\sigma_2$ | $m_3$       | $\sigma_3$ | $m_4$       | $\sigma_4$ | $m_5$      | $\sigma_5$ |
| $\Delta d$<br>(pixel)          | 0     | 0.04        | 0.04       | 0.05        | 0.03       | 0.12        | 0.06       | <b>0.08</b> | 0.05       | 0.07       | 0.06       |
|                                | 5     | 0.22        | 0.1        | 0.26        | 0.09       | 0.26        | 0.11       | <b>0.31</b> | 0.13       | 0.25       | 0.16       |
|                                | 10    | 0.33        | 0.16       | 0.41        | 0.14       | <b>0.48</b> | 0.18       | 0.34        | 0.14       | 0.42       | 0.19       |
| $\Delta\theta$<br>( $^\circ$ ) | 0     | 0.03        | 0.01       | 0.05        | 0.04       | <b>0.07</b> | 0.03       | 0.06        | 0.05       | 0.04       | 0.04       |
|                                | 5     | 0.23        | 0.14       | 0.29        | 0.17       | 0.23        | 0.21       | 0.27        | 0.15       | <b>0.3</b> | 0.08       |
|                                | 10    | 0.39        | 0.28       | 0.46        | 0.35       | 0.47        | 0.27       | <b>0.5</b>  | 0.36       | 0.32       | 0.23       |
| $\Delta l$<br>(pixel)          | 0     | 0.03        | 0.02       | <b>0.04</b> | 0.02       | 0.04        | 0.03       | 0.04        | 0.03       | 0.02       | 0.02       |
|                                | 5     | 0.11        | 0.08       | 0.12        | 0.08       | 0.13        | 0.09       | <b>0.14</b> | 0.07       | 0.13       | 0.12       |
|                                | 10    | <b>0.26</b> | 0.06       | 0.21        | 0.09       | 0.25        | 0.09       | 0.23        | 0.11       | 0.16       | 0.1        |

is 0.26 pixels, and the angle estimation accuracy is  $0.5^\circ$ . Due to the limitation of the rectangular window size of the target, we must take the decimal part of the estimated target length as an integer before carrying out local correlation positioning. Therefore, the correlation peak center positioning method proposed in this paper has subpixel-level error.

A performance comparison is not carried out in the paper. On the one hand, the target detection systems and procedures in the time domain and frequency domain are completely different and are difficult to compare fairly. On the other hand, unlike conventional object recognition, space targets in high orbits have no obvious morphological features, and what we focus on the most is the image-to-telescope feedback and the adaptability of the proposed method in different working modes of the telescope. The method can realize the separation of tracking and positioning, which is more advantageous especially when target tracking is prioritized. We can directly detect the target motion to achieve space early warnings and to guide the telescope in real time without knowledge of the target position, and the accurate motion state of the target is continuously obtained.

## V. CONCLUSION

An effective RPD method for target streaks based on motion parameter estimation is presented in this paper. We use the interframe phase difference to estimate the displacement vectors and morphological parameters of the target streak and then search for the target based on the local gray correlation in the two frames of images. This method can estimate the target streak length and position with subpixel precision in different scenes and can also solve the problem of target positioning when the target streak goes through a bright star, providing a new idea for target detection that is promising for applications in target tracking and early warning. In future work, the authors will apply the method to research on multitarget cataloging in image sequences with complex backgrounds.

## REFERENCES

- [1] Z. Tong, C. Can, F. W. Xing, H. H. Qiao, and C. H. Yu, "Improved small moving target detection method in infrared sequences under a rotational background," *Appl. Opt.*, vol. 57, no. 31, pp. 9279–9286, Oct. 2018.
- [2] J. Zuo, Z. Jia, J. Yang, and N. Kasabov, "Moving target detection based on improved Gaussian mixture background subtraction in video images," *IEEE Access*, vol. 7, pp. 152612–152623, Oct. 2019.
- [3] S. Isik, K. Özkan, S. Günel, and Ö. N. Gerek, "SWCD: A sliding window and self-regulated learning-based background updating method for change detection in videos," *J. Electron. Imag.*, vol. 27, no. 2, Apr. 2018, Art. no. 023002.
- [4] D. Zeng and M. Zhu, "Background subtraction using multiscale fully convolutional network," *IEEE Access*, vol. 6, pp. 16010–16021, Mar. 2018.
- [5] M. Wan, G. Gu, E. Cao, X. Hu, W. Qian, and K. Ren, "In-frame and inter-frame information based infrared moving small target detection under complex cloud backgrounds," *Infr. Phys. Technol.*, vol. 76, pp. 455–467, May 2016.
- [6] G. Shi, J. Suo, C. Liu, K. Wan, and X. Lv, "Moving target detection algorithm in image sequences based on edge detection and frame difference," in *Proc. IEEE 3rd Inf. Technol. Mechatronics Eng. Conf. (ITOE)*, Chongqing, China, Oct. 2017, pp. 740–744.
- [7] Z. W. Li, T. Zhang, and M. G. Sun, "Fast recognition and precise orientation of space objects in star background," *Opt. Precis. Eng.*, vol. 23, no. 2, pp. 589–599, Feb. 2015.
- [8] S. I. Young, B. Girod, and D. Taubman, "Fast optical flow extraction from compressed video," *IEEE Trans. Image Process.*, vol. 29, pp. 6409–6421, Apr. 2020.
- [9] T. Sun, F. Xing, X. Wang, J. Li, M. Wei, and Z. You, "Effective star tracking method based on optical flow analysis for star trackers," *Appl. Opt.*, vol. 55, no. 36, pp. 10335–10340, Dec. 2016.
- [10] C. Zhang, L. Ge, Z. Chen, R. Qin, M. Li, and W. Liu, "Guided filtering: Toward edge-preserving for optical flow," *IEEE Access*, vol. 6, pp. 26958–26970, Apr. 2018.
- [11] J. Hu, Y. Yu, and F. Liu, "Small and dim target detection by background estimation," *Infr. Phys. Technol.*, vol. 73, pp. 141–148, Nov. 2015.
- [12] S. Kim and J. Lee, "Scale invariant small target detection by optimizing signal-to-clutter ratio in heterogeneous background for infrared search and track," *Pattern Recognit.*, vol. 45, no. 1, pp. 393–406, Jan. 2012.
- [13] K. He, J. Sun, and X. Tang, "Guided image filtering," *IEEE Trans. Pattern Anal. Mach. Intell.*, vol. 35, no. 6, pp. 1397–1409, Jun. 2013.
- [14] Z. Li, J. Zheng, Z. Zhu, W. Yao, and S. Wu, "Weighted guided image filtering," *IEEE Trans. Image Process.*, vol. 24, no. 1, pp. 120–129, Jan. 2015.
- [15] B. J. Southwell, J. W. Cheong, and A. G. Dempster, "A matched filter for spaceborne GNSS-R based sea-target detection," *IEEE Trans. Geosci. Remote Sens.*, vol. 58, no. 8, pp. 5922–5931, Aug. 2020.
- [16] V. Alessandro, S. Klaus, and S. Thomas, "Streak detection algorithm for space debris detection on optical images," presented at the AMOS Technol. Conf., Maui, HI, USA, Sep. 2015.
- [17] V. Koupryanov, "Distinguishing features of CCD astrometry of faint GEO objects," *Adv. Space Res.*, vol. 41, no. 7, pp. 1029–1038, Jan. 2008.
- [18] A. Yang, X. Jiang, and D. D. U. Li, "Multi-frame blind deconvolution of atmospheric turbulence degraded images with mixed noise models," *Electron. Lett.*, vol. 54, no. 4, pp. 206–208, Feb. 2018.
- [19] O. Fors, J. Núñez, X. Otazu, A. Prades, and R. Cardinal, "Improving the ability of image sensors to detect faint stars and moving objects using image deconvolution techniques," *Sensors*, vol. 10, no. 3, pp. 1743–1752, Mar. 2010.

- [20] W. Zhang, S. Wang, S. Thachan, J. Chen, and Y. Qian, "Deconv R-CNN for small object detection on remote sensing images," in *Proc. IEEE Int. Geo sci. Remote Sens. Symp.*, Jul. 2018, pp. 2483–2486.
- [21] J. Núñez, A. Núñez, F. J. Montojo, and M. Condominas, "Improving space debris detection in GEO ring using image deconvolution," *Adv. Space Res.*, vol. 56, no. 2, pp. 218–228, Jul. 2015.
- [22] J. F. Khan, "Target detection in cluttered forward-looking infrared imagery," *Opt. Eng.*, vol. 44, no. 7, Jul. 2005, Art. no. 076404.
- [23] L. Deng, H. Zhu, Q. Zhou, and Y. Li, "Adaptive top-hat filter based on quantum genetic algorithm for infrared small target detection," *Multimedia Tools Appl.*, vol. 77, no. 9, pp. 10539–10551, May 2018.
- [24] M. Zeng, J. Li, and Z. Peng, "The design of top-hat morphological filter and application to infrared target detection," *Infr. Phys. Technol.*, vol. 48, no. 1, pp. 67–76, Apr. 2006.
- [25] X. Bai and F. Zhou, "Analysis of new top-hat transformation and the application for infrared dim small target detection," *Pattern Recognit.*, vol. 43, no. 6, pp. 2145–2156, Jun. 2010.
- [26] J. Jiang, L. Lei, and Z. Guangjun, "Robust and accurate star segmentation algorithm based on morphology," *Opt. Eng.*, vol. 55, no. 6, Jun. 2016, Art. no. 063101.
- [27] C. Gao, D. Meng, Y. Yang, Y. Wang, X. Zhou, and A. G. Hauptmann, "Infrared patch-image model for small target detection in a single image," *IEEE Trans. Image Process.*, vol. 22, no. 12, pp. 4996–5009, Dec. 2013.
- [28] C. L. Philip Chen, H. Li, Y. Wei, T. Xia, and Y. Yan Tang, "A local contrast method for small infrared target detection," *IEEE Trans. Geosci. Remote Sens.*, vol. 52, no. 1, pp. 574–581, Jan. 2014.
- [29] S. Erturk, "Digital image stabilization with sub-image phase correlation based global motion estimation," *IEEE Trans. Consum. Electron.*, vol. 49, no. 4, pp. 1320–1325, Nov. 2003.
- [30] Y. H. Wu and Q. Y. Yu, "An algorithm of displacement estimation by the phase-different of Fourier transform in present noise," *Opt. Precis. Eng.*, vol. 15, no. 7, pp. 1137–1142, Jul. 2007.
- [31] Y. H. Wu, J. Y. Zhao, and L. M. Zhang, "The movement estimation of target and background by Fourier transform," *Microcomput. Inf.*, vol. 26, no. 10, pp. 17–19, Apr. 2010.
- [32] S. Leonov, "Nonparametric methods for clutter removal," *IEEE Trans. Aerosp. Electron. Syst.*, vol. 37, no. 3, pp. 832–848, Jul. 2001.
- [33] Z. Li, B. Liang, T. Zhang, and H. Zhu, "Image simulation for airborne star tracker under strong background radiance," in *Proc. IEEE Int. Conf. Comput. Sci. Autom. Eng. (CSAE)*, Zhangjiajie, China, May 2012, pp. 644–648.
- [34] J. Li, Z. Liu, and F. Liu, "Using sub-resolution features for self-compensation of the modulation transfer function in remote sensing," *Opt. Exp.*, vol. 25, no. 4, pp. 4018–4037, Feb. 2017.
- [35] M.-S. Wei, F. Xing, and Z. You, "A real-time detection and positioning method for small and weak targets using a 1D morphology-based approach in 2D images," *Light, Sci. Appl.*, vol. 7, May 2018, Art. no. 18006.



**JINYU ZHAO** received the Ph.D. degree from the Changchun Institute of Optics, Fine Mechanics and Physics, Chinese Academy of Sciences, in 2006.

Since 2012, he has been a Researcher with the Changchun Institute of Optics, Fine Mechanics and Physics, Chinese Academy of Sciences. His research interests include photoelectric detection techniques and image processing.



**YUANHAO WU** received the Ph.D. degree from the Changchun Institute of Optics, Fine Mechanics and Physics, Chinese Academy of Sciences, in 2008.

He is currently an Associate Researcher with the Changchun Institute of Optics, Fine Mechanics and Physics, Chinese Academy of Sciences. His research interests include image processing and computational optics.



**BIN WANG** was born in Jilin, China, in 1980. He received the Ph.D. degree in statistics from Northeast Normal University, Changchun, China, in 2018.

He is currently a Researcher with the Changchun Institute of Optics, Fine Mechanics and Physics, Chinese Academy of Sciences. He has authored more than 20 articles. His research interests include information optics and statistical data processing.



**LEI DONG** received the Ph.D. degree from the University of Chinese Academy of Sciences, in 2019.

He is currently an Associate Researcher with the Changchun Institute of Optics, Fine Mechanics and Physics, Chinese Academy of Sciences. His research interests include optical interference imaging and detection, laser active imaging, and synthetic aperture imaging.

...



**YUNLONG ZOU** was born in Changchun, Jilin, China, in 1993. He received the B.E. degree in communication engineering from the Harbin Institute of Technology, Harbin, China, in 2016. He is currently pursuing the Ph.D. degree in optical engineering with the University of Chinese Academy of Sciences, Beijing, China.

His research interests include space target detection and image processing.